IEEE Access
Multidisciplinary ⋮ Rapid Review ⋮ Open Access Journal

Received September 4, 2021, accepted October 18, 2021, date of publication October 21, 2021, date of current version November 4, 2021.

Digital Object Identifier 10.1109/ACCESS.2021.3122010

Finite-Time Fault-Tolerant Control for a Robotic Manipulator With Output Constraint and Uncertainties

DUC THIEN TRAN[1], (Member, IEEE), AND KYOUNG KWAN AHN[2], (Senior Member, IEEE)
[1]Department of Automatic Control, Ho Chi Minh City University of Technology and Education, Ho Chi Minh City 700000, Vietnam
[2]School of Mechanical Engineering, University of Ulsan, Ulsan 44610, South Korea

Corresponding author: Duc Thien Tran (thientd@hcmute.edu.vn)

This work belongs to the project grant No: T2021-57TĐ funded by Ho Chi Minh City University of Technology and Education, Vietnam.

ABSTRACT This paper proposed a finite-time backstepping control for a robotic manipulator under the presence of actuator fault, saturation constraints, output constraints, and external disturbance to obtain requirements about the robustness, fast convergence, and high accuracy tracking performance. To manage the above challenges, the proposed control is designed on a transformed model with the backstepping approach and extended state observer. The transformed model is resulted from converting a constrained system based on a transformation technique. So, it provides an ability for the proposed control to obtain the prescribed performance of the output response. Additionally, an extended state observer is conducted to deal with the lumped uncertainties in the system. The essential characteristic of the proposed control is no required knowledge of the actuator faults and external disturbance to be available. Furthermore, fractional-order terms are added in the control laws to enhance the rate of output responses. To demonstrate the advantages of the proposed control in terms of global asymptotic stability, the Lyapunov approach is used to verify the whole controlled system in theory. The proposed control is applied to a 2-degree of freedom (DOF) manipulator and simulated by MATLAB Simulink. Its simulation results are compared to other state-of-the-art methods to exhibit the effectiveness of the proposed control.

INDEX TERMS Robotic manipulator, transformation technique, fractional-order terms, backstepping control, fault-tolerant control, output constraints, saturation constraints, external disturbance, Lyapunov approach.

I. INTRODUCTION

In recent years, robotic manipulators have been widely investigated in many applications in industrial assembly, medical assistance, warehouse, etc., because they can replace human operations in a dangerous environment and carry heavy payloads [1]. The higher performance and reliability requirements are put forward in practice. The common challenges in the robotic manipulator are disturbance/model uncertainties [2]–[4], high nonlinearity in dynamics [5], input constraints [6]–[8], and state constraints [4], [9]. In order to obtain the control requirements under the presence of the above challenges, various closed-loop controllers such as model-based feedback control [5], sliding mode control [10]–[12], backstepping control [8]–[10], [13], adaptive control [8]–[10], etc. Additionally, in modern industrial applications, faults frequently occur in the systems which operate in the condition of long-term operation [14]. So that, the robotic manipulator needs to integrate the fault-tolerant ability to ensure that the system works safely under the presence of faults in the subsystems.

In practice, the sensors and actuators are key components of the robotic manipulator system. The working environment is very complicated with vibration, electromagnetic interference, etc., which will impact the quality of the sensors and actuators. As a result, they are two common faults [15]: actuator fault and sensor faults. Otherwise, the process fault [16], which involves modeling error and external disturbance, is a different type of fault. The reliability of the robotic manipulator depends on the fault occurrence probability and fault tolerance. The fault-tolerant control schemes can be classified into two kinds: passive

The associate editor coordinating the review of this manuscript and approving it for publication was Bing Li.

fault-tolerant control (FTC) and active FTC. The passive FTC is developed as on the robust capability of the controllers such as sliding mode control (SMC) [17]–[19], adaptive control [19]–[21], etc., against the faults. The fault estimation is not needed in this approach. So, it gives a fast response when the fault happens and a simple structure. For example, Van *et al.* [18] proposed a novel control method for tracking control of robotic manipulators under the existence of the fault components, external disturbance, and viscous friction. The proposed method was developed based on a novel adaptive backstepping nonsingular fast terminal sliding mode control. The lumped uncertainties, including fault component, external disturbance, and viscous friction, were managed by adaptive techniques. Wang *et al.* [19] provided a novel adaptive integral-type terminal sliding mode fault-tolerant control for a spacecraft system regardless of the actuator fault, external disturbance, uncertainties, and actuator saturation. Adaptive laws were utilized to compensate for the lumped uncertainties. Kang and Wang [21] studied an adaptive control method for a 5-DOF upper-limb exoskeleton robot under the existence of the unknown significant parameter variances and actuator faults. In this study, an adaptive observer was implemented to provide the information for updating the adaptive controller. By contrast, the active FTC is designed based on online fault diagnosis techniques. The active FTC structure can be reconfigured based on the results of the fault diagnosis (FD) system. The active FTC owns the complicated structure and takes more time to manage the fault. But it can deal well with the high magnitude faults. The quality of the AFTC is influenced by the accuracy of the fault estimator (FE) and the system configuration after faults happen. The FE methods such as sliding mode observer [14], [22], Kalman filter [23], [24], nonlinear observer [25]–[27] have been investigated with various control strategies such as SMCs [24], [25], [27], backstepping control [28], [29], etc. In [22], a fault-tolerant control was studied for a class of descriptor stochastic systems with state-dependent faults. A novel sliding mode observer was constructed to estimate the state and faults in the system. Its results were combined with a state-feedback control to guarantee the closed-loop system was stable. In [24], Shabbouei Hagh *et al.* proposed a new hybrid robust fault-tolerant control for a 3-DOF manipulator. Two controllers, a linear robust controller in the non-fault situation and a nonsingular terminal sliding mode control in the faulty case were used with an adaptive joint unscented Kalman Filter. The Kalman filter was used for fault detection and diagnosis. To switch between two controllers, a fuzzy-based switching system was used. In [25], Van *et al.* applied a novel finite time fault-tolerant control for uncertain robot manipulators with actuator faults. The proposed control includes a nonsingular fast terminal sliding mode control with a simple fault diagnosis which is established based on time delay estimation. In [28], an active fault-tolerant control was proposed for a class of uncertain SISO nonlinear flight control systems. The proposed method was developed based on the adaptive observer, feedback linearization, and backstepping theory. The fault in the faulty system is estimated by an adaptive observer. The effectiveness of the proposed method was evaluated both in theory and in simulation. Based on the above analysis, the previous studies have considered the tracking objectives for the systems under the presence of the modeling error, external disturbance, or input constraints besides the fault occurrences. In recent years, the output constraint problems in manipulators have been interesting to many researchers around the world. To the best of the authors' knowledge, there are only a few studies, which consider these issues in the FTC design.

The output constraints are restrictions of the output responses, which are produced by the output signals of the trajectory planning and environmental information. They usually happen when the robot operates near or with humans in applications such as polishing, deburring, assembly, etc., or working in narrow environments. The role of the output constraints is to guarantee the satisfaction of constraint requirements, accuracy, and safety of both humans and robots. Some techniques have been conducted comprising of transforming approach [30]–[32] and barrier Lyapunov function (BLF) [33]–[35] to handle the performance constraints problem. The BLF was first presented to cope with the constant output constraint problem [30] in 2009. The BLF was proposed for nonlinear systems with the presence of output constraints [36] and full state constraints [37]. Because of the complication of the BLFs, it is hard to use this approach for designing and analyzing advanced controllers, in which finite-time convergence is expected. The transforming method called prescribed performance control was presented in [38], which can deal with the performance constraints by converting the constrained system into the unconstrained system. On the other hand, the transformed system possesses potential properties for employing a controller to cope with finite-time convergence issues.

Additionally, when actuator faults happen, the input saturation issue will arise and is another critical problem that needs to be addressed in control design. Because of the physical limitations in the actuator, it cannot produce the typically commanded control input. When the actuator faults happen, the control signal of the other actuators will be increased to compensate for the faulty actuators and maintain the control performance of the control system. So, the actuator faults can cause input saturation issues which further produce some physical dynamics and even instability in the control system.

In this paper, a novel finite-time backstepping control is proposed for prescribed tracking performances of manipulators under the presence of the actuator faults, input constraints, and external disturbances. To manage the above challenges, the proposed control design is conducted based on the transformed model, which is generated by using the transformation error technique to integrate the prescribed performance, called output constraint, into the manipulator dynamics. Then, the backstepping control with fraction order

terms is conducted to ensure tracking problems and to enhance the transient response. To deal with the external disturbance and actuator faults, an extended state observer is equipped in the finite backstepping control to generate the final version of the proposed control. To prove the stability and robustness of the proposed control against the challenges, in theory, a Lyapunov approach is used to analyze the whole controlled system. Finally, the proposed control is applied on a 2-DOF manipulator with MATLAB Simulink. The comparisons of its results with other methods will demonstrate the effectiveness of the proposed control.

This paper is organized as follows: Section II presents manipulator dynamics with the challenges, transformation techniques, and extended state observer. In Section III, the proposed control and its stability analysis are exhibited. In Section IV, some simulation results are discussed to show the effectiveness of the proposed control. Finally, some conclusions and future works are summarized.

II. PROBLEM DESCRIPTION

A. PRELIMINARIES

Lemma 1 ([39]): When the continuous positive definite function

$$\dot{V}(t) \leq -a_1 V(t) - a_2 V^b(t) + \eta, \forall t \geq t_0, V(t_0) \geq 0 \quad (1)$$

where $a_{i(i=1,2)}$ are positive constants, b is a ratio of two odd positive integers with $0 \leq b \leq 1$, and $0 < \eta < \infty$, then the function $V(t)$ converges to zero in finite time, T_f, with any given time t_0.

$$\lim_{t \to t_0} V(t) \leq \min\left(\frac{\eta}{(1-\theta_0)\, a_1}, \left(\frac{\eta}{(1-\theta_0)\, a_2}\right)^{\frac{1}{b}}\right) \quad (2)$$

where $0 < \theta_0 < 1$. The finite time is calculated as follows:

$$T_f \leq \max\left(t_0 + \frac{1}{\theta_0 a_1 (1_0 - b)} \ln \frac{\theta_0 a_1 V^{1-b}(t_0) + a_2}{a_2}, t_0 + \frac{1}{a_1 (1-b)} \ln \frac{a_1 V^{1-b}(t_0) + \theta_0 a_2}{\theta_0 a_2}\right) \quad (3)$$

Notion 1: Some definitions used throughout this paper are presented as follows:

$$\xi^c = |\xi|^c \, sign(\xi) \quad (4)$$

where $c > 0$. Some vector definitions are presented as follows:

$$\boldsymbol{\xi} = [\xi_1, \ldots, \xi_n]^T \in R^{n\times 1} \quad (5)$$

$$\boldsymbol{\xi}^c = |\boldsymbol{\xi}|^c \, \mathbf{sgn}(\boldsymbol{\xi}) = \left[|\xi_1|^c \, sign(\xi_1), \ldots, |\xi_n|^c \, sign(\xi_n)\right] \in R^{n\times 1} \quad (6)$$

$$|\boldsymbol{\xi}|^c = diag\left(\left[|\xi_1|^c, \ldots, |\xi_n|^c\right]\right) \in R^{n\times n} \quad (7)$$

$$\mathbf{sgn}(\boldsymbol{\xi}) = [sign(\xi_1), \ldots, sign(\xi_n)]^T \in R^{n\times 1} \quad (8)$$

Lemma 2 ([40]): For any real number y_i, $i = 1, \ldots, n$ if $0 < b_1 < 1$ and $0 < b_2 < 2$ then the following inequality hold:

$$(|y_1| + \ldots + |y_n|)^{b_1} \leq |y_1|^{b_1} + \ldots + |y_n|^{b_1} \quad (9)$$

$$\left(|y_1|^2 + \ldots + |y_n|^2\right)^{b_2} \leq \left(|y_1|^{b_2} + \ldots + |y_n|^{b_2}\right)^2 \quad (10)$$

B. MANIPULATOR DYNAMICS

This study focuses on considering an n-DOF manipulator under the presence of the actuator faults, input/output constraints, and external disturbance. The manipulator dynamics are presented by derivative formulation of the form [5]

$$\mathbf{M}(\mathbf{q})\ddot{\mathbf{q}} + \mathbf{C}(\mathbf{q}, \dot{\mathbf{q}})\dot{\mathbf{q}} + \mathbf{G}(\mathbf{q}) + \mathbf{d}(t) = \boldsymbol{\tau} \quad (11)$$

where $\mathbf{q}, \dot{\mathbf{q}}$, and $\ddot{\mathbf{q}} \in R^{n\times 1}$ respectively derive position, angular velocity, and angular acceleration vectors of each joint; $\mathbf{M}(\mathbf{q}) \in R^{n\times n}$ derives the symmetric and positive definite inertia matrix; $\mathbf{C}(\mathbf{q}, \dot{\mathbf{q}}) \in R^{n\times n}$ presents the matrix of Coriolis and Centrifugal force; $\mathbf{G}(\mathbf{q}) \in R^{n\times 1}$ denotes the gravitational vector; $\boldsymbol{\tau} \in R^{n\times 1}$ presents the control input vector; $\mathbf{d}(t) = \mathbf{J}^{\mathbf{T}}(\mathbf{q})\mathbf{f}_{ext} \in R^{n\times 1}$ is the external torque; $\mathbf{J}(\mathbf{q}) \in R^{n\times n}$ presents a nonsingular Jacobian matrix; $\mathbf{f}_{ext} \in R^{n\times 1}$ exhibits the external disturbance force at the end-effector.

Assumption 1: The external disturbances and unknown friction functions are bounded functions.

C. ACTUATOR FAULTS

In practice, the actuator can be separated into four categories: loss effectiveness, clocked-in-place, floating around trim, and hard over. In the n-DOF manipulator, n actuators are used to control the system. The four categories of actuator fault are exhibited as follows:

$$\boldsymbol{\tau} = \boldsymbol{\alpha}\mathbf{u} + \tilde{\mathbf{u}} \in R^{n\times 1} \quad (12)$$

where $\boldsymbol{\tau} \in R^{n\times 1}$ is the applied control, $\mathbf{u} = [u_1, \ldots, u_n]^T \in R^{n\times 1}$ presents the control input commanded by the controllers, $\boldsymbol{\alpha} = diag\left([\alpha_1, \ldots, \alpha_n]^T\right) \in R^{n\times n}$ is the actuator effectiveness matrix, $\tilde{\mathbf{u}} \in R^{n\times 1}$ is the uncertain fault.

D. INPUT SATURATION

Because of the physical and electrical limitations in actuators, the control signals are restricted by saturation values. The saturation control signal of the manipulator is defined as follows:

$$sat(u_i) = \begin{cases} u_{mi} sign(u_i), & |u_i| > u_{mi} \\ u_i, & |u_i| \leq u_{mi} \end{cases} \quad (13)$$

where u_{mi} is the maximum value of the i$^{\text{th}}$ control input.

The equation (13) can be represented as follows:

$$\mathbf{sat}(\mathbf{u}) = \mathbf{u} + \Delta\mathbf{u} \quad (14)$$

where $\mathbf{sat}(u) = [sat(u_1), \ldots, sat(u_n)]^T \in R^{n\times 1}$ is saturation control input vector, $\Delta\mathbf{u} = [\Delta u_1, \ldots, \Delta u_n]^T \in R^{n\times 1}$ presents the excess vector of the input constrains.

$$\Delta u_i = \begin{cases} 0, & |u_i| < u_{mi} \\ u_{mi} sign(u_i) - u_i, & |u_i| \geq u_{mi} \end{cases} \quad (15)$$

Remark 1: Because of the physical and electrical limitations on the actuators, the practical control torque produced by the actuator is restricted. Additionally, the excess limited saturation input $\Delta\mathbf{u}$ and the additive fault $\tilde{\mathbf{u}}$ are also bounded.

The manipulator dynamics can be rewritten by integrating the actuator fault and input saturation. It yields as follows:

$$\mathbf{M}(\mathbf{q})\ddot{\mathbf{q}} + \mathbf{C}(\mathbf{q}, \dot{\mathbf{q}})\dot{\mathbf{q}} + \mathbf{G}(\mathbf{q}) + \Delta\mathbf{d}(t) = \mathbf{u} \tag{16}$$

where $\Delta\mathbf{d}(t) = \mathbf{d}(t) - \tilde{\mathbf{u}} + (1-\alpha)\mathbf{u} - \Delta\mathbf{u}$ are the lumped uncertainties consisting of external disturbance, actuator fault, and excess constrained term.

Let define $x_1 = q \in R^{n\times 1}$, $x_2 = \dot{q} \in R^{n\times 1}$, the uncertain manipulator dynamics (16) can be expressed as follows

$$\begin{cases} \dot{\mathbf{x}}_1 = \mathbf{x}_2 \\ \dot{\mathbf{x}}_2 = \mathbf{M}^{-1}(\mathbf{x}_1)\left[\mathbf{u} - \mathbf{C}(\mathbf{x}_1, \mathbf{x}_2)\mathbf{x}_2 - \mathbf{G}(\mathbf{x}_1) - \Delta\mathbf{d}(t)\right] \end{cases} \tag{17}$$

E. EXTENDED STATE OBSERVER

In order to estimate the lumped uncertainties, an extended state observer (ESO) is investigated in the manipulator dynamics (16). Additionally, an extra state x_3 is defined to exhibit the lumped uncertainties, $\mathbf{M}^{-1}(x_1)\Delta\mathbf{d}(t)$.

Now, the robotic manipulator dynamics (17) is represented as follows:

$$\begin{cases} \dot{\mathbf{x}}_1 = \mathbf{x}_2 \\ \dot{\mathbf{x}}_2 = \mathbf{H}(\mathbf{x}_1, \mathbf{x}_2) + \mathbf{B}(x_1)\mathbf{u} + \mathbf{x}_3 \\ \dot{\mathbf{x}}_3 = \boldsymbol{\delta}(t) \end{cases} \tag{18}$$

where $\mathbf{x}_3 = -\mathbf{M}^{-1}(\mathbf{x}_1)\Delta\mathbf{d}(t) \in R^{n\times 1}$, $\mathbf{B}(\mathbf{x}_1) = \mathbf{M}^{-1}(\mathbf{x}_1) \in R^{n\times n}$, $\mathbf{H}(\mathbf{x}_1, \mathbf{x}_2) = -\mathbf{M}^{-1}(\mathbf{x}_1)(\mathbf{C}(\mathbf{x}_1, \mathbf{x}_2)\mathbf{x}_2 + \mathbf{G}(\mathbf{x}_1)) \in R^{n\times 1}$, and $\boldsymbol{\delta}(t) \in R^{n\times 1}$ is the derivative of $\mathbf{x}_3$.

Assumption 2: Based on Assumption 1 and Remark 1, the lumped uncertainties are bounded. Furthermore, the time derivative of the state $\mathbf{x}_3(t)$ is supposed to be bounded.

The ESO is designed as follows:

$$\begin{cases} \dot{\hat{\mathbf{x}}}_1 = \hat{\mathbf{x}}_2 + \boldsymbol{\sigma}_1(\mathbf{x}_1 - \hat{\mathbf{x}}_1) \\ \dot{\hat{\mathbf{x}}}_2 = \mathbf{H}(\hat{\mathbf{x}}_1, \hat{\mathbf{x}}_2) + \mathbf{B}(\hat{x}_1)\mathbf{u} + \hat{\mathbf{x}}_3 + \boldsymbol{\sigma}_2(\mathbf{x}_1 - \hat{\mathbf{x}}_1) \\ \dot{\hat{\mathbf{x}}}_3 = \boldsymbol{\sigma}_3(\mathbf{x}_1 - \hat{\mathbf{x}}_1) \end{cases} \tag{19}$$

where $\hat{x}_i\ (i = 1, 2, 3) \in R^{n\times 1}$ is estimated state variables of the ESO, $\boldsymbol{\sigma}_1 = 3diag([\sigma_{01}, \sigma_{02}])$, $\boldsymbol{\sigma}_2 = 3diag([\sigma_{01}^2, \sigma_{02}^2])$ and $\boldsymbol{\sigma}_1 = diag([\sigma_{01}^3, \sigma_{02}^3])$ are observer matrices.

To move on, the following Lemma 3 is introduced to present the proof of stability analysis of the ESO, which can be found in [40].

Lemma 3 ([41]): when the manipulator system (18) and the ESO (19) are considered with a suitable observer gain, β_0, the estimated results, $\hat{\mathbf{x}}_i\ (i = 1, 2, 3)$, of the ESO (19) will track the state responses, $\mathbf{x}_i\ (i = 1, 2, 3)$ in the system (18).

F. OUTPUT CONSTRAINTS

For the output tracking error, $e_1 = x_1 - x_{1d} \in R^{n\times 1}$, it will obtain the predefined performance if the errors satisfy the below conditions:

$$-\sigma_{1i}\mu(t) < e_{1i}(t) < \sigma_{2i}\mu(t) \tag{20}$$

where $0 < \sigma_{ji(j=1,2;i=1,\ldots,n)} \leq 1$ are positive constants, and $\mu(t)$ is a predefined performance. The function $\mu(t)$ is selected as follows:

$$\mu(t) = (\mu_0 - \mu_\infty)\exp(-\kappa_f t) + \mu_\infty \tag{21}$$

where μ_0 is an initial value of $\mu(t)$, $\mu_\infty = \lim_{t\to\infty}\mu(t) > 0$ and κ_f is a positive constant.

Remark 2: The initial value of $\mu(t)$ is selected how the conditions, $-\sigma_{1i}\mu_0 < e_{1i}(0) < \sigma_{2i}\mu_0$, are satisfied.

In order to integrate the errors, $e_{1i}(t)$ with their predefined performance, a nonlinear transformation [32] scheme is conducted as follows

$$e_{1i}(t) = \sigma_{2i}\mu(t)\Phi_i(z_i(t), \eta_i) \tag{22}$$

where $\eta_i = -\sigma_{1i}/\sigma_{2i}$, z_i is the new error variable, $\Phi_i(.)$ is an increasing and invertible function with respect to $z_i(t)$, $\Phi_i(z_i(t), \eta_i) = \frac{e^{z_i} + \eta_i e^{-z_i}}{e^{z_i} + e^{-z_i}}$, which satisfies the following conditions

$$\begin{aligned} \lim_{z_i(t)\to-\infty}(\Phi_i(z_i(t), \eta_i)) &= \eta_i \\ \lim_{z_i(t)\to+\infty}(\Phi_i(z_i(t), \eta_i)) &= 1 \end{aligned} \tag{23}$$

Now, the new error variable, $z_i(t)$, can be computed as

$$z_i(t) = \Phi_i^{-1}\left(\frac{e_{1i}(t)}{\sigma_{2i}\mu(t)}, \eta_i\right) = \frac{1}{2}\ln\frac{e_i(t) + \sigma_1\mu(t)}{\sigma_{2i}\mu(t) - e_i(t)} \tag{24}$$

Remark 3: When the new variable $z_i(t)$ is bounded, the following inequality holds:

$$\eta_i < \Phi_i(z_i(t), \eta_i) < 1 \tag{25}$$

By multiplying $\sigma_{2i}\mu(t)$ in three sides of Eq. (25), its result is presented as follows:

$$-\sigma_{1i}\mu(t) < \sigma_{2i}\mu(t)\Phi_i(z_i(t), \eta_i) = e_{1i}(t) < \sigma_{2i}\mu(t) \tag{26}$$

which implied that the output responses are bounded by the output constraints, as shown in (20).

The differentiating $z_i(t)$ with respect to time is calculated as follows:

$$\dot{z}_i = \frac{\partial\Phi_i^{-1}}{\partial\left(\frac{e_{1i}(t)}{\bar{e}_{1i}(t)}\right)}\frac{1}{\bar{e}_{1i}(t)}\left(\dot{e}_{1i}(t) - e_{1i}(t)\frac{\dot{\bar{\mu}}(t)}{\mu(t)}\right) \tag{27}$$

where $\bar{e}_{1i}(t) = \sigma_{2}\mu(t)$.

By integrating the predefined responses into the manipulator dynamics (17), an unconstrained dynamics is presented as follows:

$$\begin{aligned} \dot{\mathbf{z}} &= \mathbf{H}\mathbf{x}_2 + \boldsymbol{\Psi} \\ \dot{\mathbf{x}}_2 &= \mathbf{M}^{-1}(\mathbf{x}_1)(\mathbf{u} - \mathbf{C}(\mathbf{x}_1, \mathbf{x}_2)\mathbf{x}_2 - \mathbf{G}(\mathbf{x}_1) - \Delta\mathbf{d}(t)) \end{aligned} \tag{28}$$

where

$$\mathbf{H} = diag\left(\left[\frac{\partial\Phi_1^{-1}}{\partial\left(\frac{e_{11}}{\bar{e}_{11}}\right)}\frac{1}{\bar{e}_{11}} \cdots \frac{\partial\Phi_n^{-1}}{\partial\left(\frac{e_{1n}}{\bar{e}_{1n}}\right)}\frac{1}{\bar{e}_{1n}}\right]\right) \in R^{n\times n} \tag{29}$$

$$\boldsymbol{\Psi} = -\mathbf{H}\left(\dot{\mathbf{x}}_d + \frac{\dot{\bar{\mu}}(t)}{\mu(t)}\mathbf{e}_1\right) \in R^{n\times 1} \tag{30}$$

III. PROPOSED METHOD

A. CONTROL DESCRIPTION

The objectives of the proposed control are to guarantee that the output responses of the n-DOF manipulator not only track the trajectories but also stay inside the predefined boundary around the trajectory while the manipulator operates under the presence of the input saturation, actuator faults, and external disturbance. As analyzed in Section II, the excessed term and faults in the actuator and external disturbance are presented by the lumped uncertainties, $\Delta\mathbf{d}(t)$. By using the external state observer, the lumped uncertainties can be approximated and provided for the finite time backstepping control. The proposed control insists on finite time backstepping control and ESO (FTBCESO) is named as finite-time fault-tolerant control. Additionally, because the proposed control is designed on unconstrained dynamics (28), it can ensure that the output responses satisfy the predefined output constraints. The structure of the proposed control is presented in FIGURE 1.

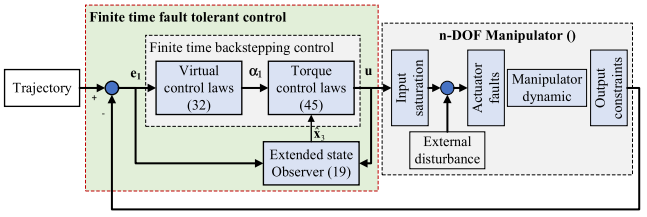

FIGURE 1. Structure of the finite-time fault-tolerant control.

B. A FINITE TIME BACKSTEPPING CONTROL DESIGN

1) CONTROL DESIGN

The tracking errors in the unconstrained system (28) are defined as follows:

$$\begin{aligned}\mathbf{e}_z &= \mathbf{z}\\ \mathbf{e}_2 &= \mathbf{x}_2 - \boldsymbol{\alpha}_1 \in R^{n\times 1}\end{aligned} \tag{31}$$

where $\boldsymbol{\alpha}_1 \in R^{n\times 1}$ presents the virtual control vector.

The virtual control vector is selected as follows:

$$\boldsymbol{\alpha}_1 = \mathbf{H}^{-1}\left(-\mathbf{K}_{10}\mathbf{e}_z - \mathbf{K}_{11}\mathbf{e}_z^{\beta_2} - \boldsymbol{\Psi}\right) \tag{32}$$

where $\mathbf{K}_{10} \in R^{n\times n}$ and $\mathbf{K}_{11} \in R^{n\times n}$ are positive diagonal matrices; $0 < \beta_2 < 1$ is a positive constant.

The control law is chosen as follows:

$$\begin{aligned}\mathbf{u}(t) = -\mathbf{H}\mathbf{e}_z - \mathbf{K}_{20}\mathbf{e}_2 - \mathbf{K}_{21}\mathbf{e}_2^{\beta_2} + \mathbf{C}(\mathbf{x}_1,\mathbf{x}_2)\boldsymbol{\alpha}_1\\ +\mathbf{G}(\mathbf{x}_1) + \mathbf{M}\dot{\boldsymbol{\alpha}}_1\end{aligned} \tag{33}$$

where $\mathbf{K}_{2i} \in R^{n\times n}$ $(i = 0, 1)$ are positive diagonal matrices.

The time derivative of the new variable error, $\mathbf{e}_z$, is calculated as follows:

$$\dot{\mathbf{e}}_z = \dot{\mathbf{z}} = \mathbf{H}\mathbf{x}_2 + \boldsymbol{\Psi} = \mathbf{H}(\mathbf{e}_2 + \boldsymbol{\alpha}_1) + \boldsymbol{\Psi} \tag{34}$$

By replacing the virtual control (32) into (34), its result is presented as follows:

$$\dot{\mathbf{e}}_z = \mathbf{H}\mathbf{e}_2 - \mathbf{K}_{10}\mathbf{e}_z - \mathbf{K}_{11}\mathbf{e}_z^{\beta_2} \tag{35}$$

Next, the differential of the velocity error with respect to time is calculated as follows:

$$\begin{aligned}\dot{\mathbf{e}}_2 &= \dot{\mathbf{x}}_2 - \dot{\boldsymbol{\alpha}}_1\\ &= \mathbf{M}^{-1}(\mathbf{x}_1)\left(\mathbf{u} - \mathbf{C}(\mathbf{x}_1,\mathbf{x}_2)\mathbf{x}_2 - \mathbf{G}(\mathbf{x}_1) - \Delta\mathbf{d}(t)\right) - \dot{\boldsymbol{\alpha}}_1\end{aligned} \tag{36}$$

By substituting the control law (33) into (36), it yields as follows:

$$\begin{aligned}\dot{\mathbf{e}}_2 = \mathbf{M}^{-1}(\mathbf{x}_1)\\ \times\left(-\mathbf{H}\mathbf{e}_z - \mathbf{K}_{20}\mathbf{e}_2 - \mathbf{K}_{21}\mathbf{e}_2^{\beta_2} - \mathbf{C}(\mathbf{x}_1,\mathbf{x}_2)\mathbf{e}_2 - \Delta\mathbf{d}(t)\right)\end{aligned} \tag{37}$$

Theorem 1: When the finite time backstepping control laws in (32) and (33) are conducted on a manipulator whose dynamics is presented in (17) with the input saturation, actuator fault, external disturbance, and output constraint, it guarantees not only the finite-time stability of the controlled system but also the output constraints of the output responses. The residual set of the manipulator dynamics is set by

$$\lim_{t-T_r}|V_2(e) \le \min\left\{\frac{\varphi}{(1-\theta_0)\kappa_1}, \left(\frac{\varphi}{(1-\theta_0)\kappa_2}\right)^{\frac{2}{1+\beta_2}}\right\} \tag{38}$$

where $0 < \theta_0 < 1$;

$$\begin{aligned}\kappa_1 &= \min\left\{\lambda_{\min}(K_{10}), \lambda_{\min}\left(\left(K_{20} - \frac{1}{2}I_{n\times n}\right)M^{-1}\right)\right\},\\ \kappa_2 &= \min\left\{\lambda_{\min}(\mathbf{K}_{11}), \lambda_{\min}\left(\mathbf{K}_{21}\mathbf{M}^{-\frac{(1+\beta_2)}{2}}\right)\right\},\end{aligned}$$

and $\varphi = \frac{1}{2}\left\|\Delta\mathbf{d}^T\Delta\mathbf{d}\right\|_\infty$, $\mathbf{e} = \left[\mathbf{e}_z^T \;\; \mathbf{e}_2^T\right]^T$. The finite time is

$$T_r \le \max\left\{\begin{array}{l} t_0 + \dfrac{2}{\theta_0(1-\beta_2)}\ln\dfrac{\theta_0\kappa_1 V^{\frac{1+\beta_2}{2}}(e(t_0)) + \kappa_2}{\kappa_2},\\ t_0 + \dfrac{2}{\kappa_1(1-\beta_2)}\ln\dfrac{\kappa_1 V^{1-\beta_2}(e(t_0)) + \theta_0\kappa_2}{\theta_0\kappa_2}\end{array}\right\} \tag{39}$$

where t_0 is the initial time, and $\lambda_{\min}(.)$ is minimum of eigenvalues.

To demonstrate the stability of Theorem 1, a Lyapunov function is selected as follows:

$$V_2 = V_1 + \frac{1}{2}\mathbf{e}_2^T\mathbf{M}\mathbf{e}_2 \tag{40}$$

where $V_1 = \frac{1}{2}\mathbf{e}_z^T\mathbf{e}_z$.

2) PROOF OF THEOREM 1

By taking the time derivative of the function, V_1, it yields as follows:

$$\dot{V}_1 = \mathbf{e}_z^T\dot{\mathbf{e}}_z = \mathbf{e}_z^T\left(\mathbf{H}\mathbf{e}_2 - \mathbf{K}_{10}\mathbf{e}_z - \mathbf{K}_{11}\mathbf{e}_z^{\beta_2}\right) \tag{41}$$

Thus, the differential of the Lyapunov function (40) with respect to time is calculated as follows:

$$\begin{aligned}\dot{V}_2 &= \dot{V}_1 + \mathbf{e}_2^T\mathbf{M}\dot{\mathbf{e}}_2 + \frac{1}{2}\mathbf{e}_2^T\dot{\mathbf{M}}\mathbf{e}_2 \\ &= \mathbf{e}_z^T\left(\mathbf{H}\mathbf{e}_2 - \mathbf{K}_{10}\mathbf{e}_z - \mathbf{K}_{11}\mathbf{e}_z^{\beta_2}\right) + \mathbf{e}_2^T\mathbf{M}\dot{\mathbf{e}}_2 + \frac{1}{2}\mathbf{e}_2^T\dot{\mathbf{M}}\mathbf{e}_2\end{aligned} \tag{42}$$

When Eq. (37) is replaced into (42), its result is expressed as follows:

$$\begin{aligned}\dot{V}_2 &= \mathbf{e}_z^T\left(\mathbf{H}\mathbf{e}_2 - \mathbf{K}_{10}\mathbf{e}_z - \mathbf{K}_{11}\mathbf{e}_z^{\beta_2}\right) + \frac{1}{2}\mathbf{e}_2^T\dot{\mathbf{M}}\mathbf{e}_2 \\ &\quad + \mathbf{e}_2^T\left(-\mathbf{H}\mathbf{e}_z - \mathbf{K}_{20}\mathbf{e}_2 - \mathbf{K}_{21}\mathbf{e}_2^{\beta_2}\right. \\ &\quad \left. - \mathbf{C}\left(\mathbf{x}_1, \mathbf{x}_2\right)\mathbf{e}_2 - \Delta\mathbf{d}\left(t\right)\right) \\ &= -\mathbf{e}_z^T\left(\mathbf{K}_{10}\mathbf{e}_z + \mathbf{K}_{11}\mathbf{e}_z^{\beta_2}\right) - \mathbf{e}_2^T\left(\mathbf{K}_{20}\mathbf{e}_2 + \mathbf{K}_{21}\mathbf{e}_2^{\beta_2}\right) \\ &\quad + \mathbf{e}_2^T\Delta\mathbf{d}\left(t\right)\end{aligned} \tag{43}$$

By applying Young's inequation, $\mathbf{e}_2^T\Delta\mathbf{d}\left(t\right) \leq \frac{1}{2}\left(e_2^T e_2 + \Delta\mathbf{d}^T\Delta\mathbf{d}\right)$ and Lemma 2 into the Eq. (43), its result can be derived as follows:

$$\begin{aligned}\dot{V}_2 &\leq -\mathbf{e}_z^T\left(\mathbf{K}_{10}\mathbf{e}_z + \mathbf{K}_{11}\mathbf{e}_z^{\beta_2}\right) \\ &\quad -\mathbf{e}_2^T\left(\left(\mathbf{K}_{20} - \frac{1}{2}\mathbf{I}_{n\times n}\right)\mathbf{e}_2 + \mathbf{K}_{21}\mathbf{e}_2^{\beta_2}\right) \\ &\quad + \frac{1}{2}\Delta\mathbf{d}^T\Delta\mathbf{d} \\ &= -\mathbf{e}_z^T\mathbf{K}_{10}\mathbf{e}_z - \mathbf{e}_2^T\left(\mathbf{K}_{20} - \frac{1}{2}\mathbf{I}_{n\times n}\right)\mathbf{e}_2 - \mathbf{e}_z^T\mathbf{K}_{11}\mathbf{e}_z^{\beta_2} \\ &\quad -\mathbf{e}_2^T\mathbf{K}_{21}\mathbf{e}_2^{\beta_2} \\ &\quad + \frac{1}{2}\Delta\mathbf{d}^T\Delta\mathbf{d} \\ &\leq -\kappa_1 V_2 - \kappa_2 V_2^{\beta_2} + \varphi\end{aligned} \tag{44}$$

where $\kappa_1 = \min\left\{\lambda_{\min}\left(K_{10}\right), \lambda_{\min}\left(\left(K_{20} - \frac{1}{2}I_{n\times n}\right)M^{-1}\right)\right\}$, $\kappa_2 = \min\left\{\lambda_{\min}\left(\mathbf{K}_{11}\right), \lambda_{\min}\left(\mathbf{K}_{21}\mathbf{M}^{-\frac{(1+\beta_2)}{2}}\right)\right\}$, and $\varphi = \frac{1}{2}\left\|\Delta\mathbf{d}^T\Delta\mathbf{d}\right\|_\infty$.

From (44) and Lemma 1, the stability and finite-time convergence of the controlled system are guaranteed. Furthermore, it also ensures the output responses will satisfy the output constraints as the state in **Remark 3**. So, Theorem 1 is demonstrated.

Remark 4: Although the stability, finite-time convergence, and output constraints of the controlled system are obtained with the finite-time backstepping control, the accuracy of the controlled system can be influenced by the lumped uncertainties. As a result, the significant uncertainties can make the output responses break the predefined performances, which implies the unsatisfaction of the output constraints. To enhance the accuracy and guarantee the satisfaction of the output constraints, an ESO is utilized to deal with the uncertainties. The control design will be presented in Section III.C.

C. PROPOSED CONTROL DESIGN

The proposed control laws are selected as follows:

$$\begin{aligned}\boldsymbol{\alpha}_1 &= \mathbf{H}^{-1}\left(-\mathbf{K}_{10}\mathbf{e}_z - \mathbf{K}_{11}\mathbf{e}_z^{\beta_2} - \boldsymbol{\Psi}\right) \\ \mathbf{u}\left(t\right) &= -\mathbf{H}\mathbf{e}_z - \mathbf{K}_{20}\mathbf{e}_2 - \mathbf{K}_{21}\mathbf{e}_2^{\beta_2} + \mathbf{C}\left(\mathbf{x}_1, \mathbf{x}_2\right)\boldsymbol{\alpha}_1 \\ &\quad + \mathbf{G}\left(\mathbf{x}_1\right) + \mathbf{M}\dot{\boldsymbol{\alpha}}_1 - \mathbf{M}\hat{\mathbf{x}}_3\end{aligned} \tag{45}$$

With the ESO (19) is used to approximate the lumped uncertainties, $\hat{\mathbf{x}}_3$.

Now, the time derivative of the velocity error (37) is represented as follows:

$$\begin{aligned}\dot{\mathbf{e}}_2 = \mathbf{M}^{-1}\left(\mathbf{x}_1\right)\left(-\mathbf{H}\mathbf{e}_z - \mathbf{K}_{20}\mathbf{e}_2 - \mathbf{K}_{21}\mathbf{e}_2^{\beta_2} - \mathbf{C}\left(\mathbf{x}_1, \mathbf{x}_2\right)\mathbf{e}_2\right. \\ \left. -\mathbf{M}\hat{\mathbf{x}}_3 - \Delta\mathbf{d}\right)\end{aligned} \tag{46}$$

Theorem 2: Under Assumption 1 and 2, the proposed control laws (45), the ESO (19), and the output constraints (20) are applied for the robotic manipulator (11) under the presence of the input saturation, actuator faults, and external disturbances. The proposed control will guarantee that the whole controlled system is uniformly ultimately bounded stable. The tracking error will stay in an arbitrarily small region with suitable control parameters. Furthermore, the output responses always satisfy the predefined output constraints.

Proof of Theorem 2:

Remark 5: When the ESO (19) is provided for estimating the lumped uncertainties with the suitable parameters, the estimation error of ESO, $\mathbf{M}\mathbf{x}_3 - \Delta\mathbf{d}$, can be made arbitrarily small. The total approximated error is expressed as follows

$$\varepsilon = \left\|\mathbf{M}\hat{\mathbf{x}}_3 - \Delta\mathbf{d}\right\|_\infty \tag{47}$$

With the proposed control laws (45), the result of time derivative of the Lyapunov candidate (43) have some modifications as follows:

$$\begin{aligned}\dot{V}_2 = -\mathbf{e}_z^T\left(\mathbf{K}_{10}\mathbf{e}_z + \mathbf{K}_{11}\mathbf{e}_z^{\beta_2}\right) - \mathbf{e}_2^T\left(\mathbf{K}_{20}\mathbf{e}_2 + \mathbf{K}_{21}\mathbf{e}_2^{\beta_2}\right) \\ -\mathbf{e}_2^T\left(\mathbf{M}\hat{\mathbf{x}}_3 - \Delta\mathbf{d}\right)\end{aligned} \tag{48}$$

By applying Young's inequation and (47) for $-\mathbf{e}_2^T\left(\mathbf{M}\hat{\mathbf{x}}_3 - \Delta\mathbf{d}\right)$, the Eq. (48) is expressed as follows:

$$\begin{aligned}\dot{V}_2 &\leq -\mathbf{e}_z^T\left(\mathbf{K}_{10}\mathbf{e}_z + \mathbf{K}_{11}\mathbf{e}_z^{\beta_2}\right) - \mathbf{e}_2^T\left(\mathbf{K}_{20}\mathbf{e}_2 + \mathbf{K}_{21}\mathbf{e}_2^{\beta_2}\right) \\ &\quad + \frac{1}{2}\mathbf{e}_2^T\mathbf{e}_2 + \frac{1}{2}\varepsilon^2 \\ &= -\mathbf{e}_z^T\left(\mathbf{K}_{10}\mathbf{e}_z + \mathbf{K}_{11}\mathbf{e}_z^{\beta_2}\right) \\ &\quad -\mathbf{e}_2^T\left(\left(\mathbf{K}_{20} - \frac{1}{2}\mathbf{I}_{n\times n}\right)\mathbf{e}_2 + \mathbf{K}_{21}\mathbf{e}_2^{\beta_2}\right) \\ &\quad + \frac{1}{2}\varepsilon^2 \\ &\leq -\kappa_1 V_2 - \kappa_2 V_2 + \varphi\end{aligned} \tag{49}$$

Now, φ is defined as $\varphi = \frac{1}{2}\varepsilon^2$.

From (49) and Lemma 2, we can affirm that all error variables are uniformly ultimately bounded with finite-time convergence. The finite time is presented in (39).

Furthermore, the accuracy of the controlled system is also improved by the estimated results of the ESO. Thus, Theorem 2 is proven.

Remark 6: The control gains, $\mathbf{K}_{ij}$ $(i = 1, 2; j = 0, 1)$, in the proposed control are selected how to make sure that the constants, κ_i $(i = 1, 2)$, are positive.

IV. SIMULATION

To evaluate further the advantages of the proposed control, some simulations are conducted for a 2-DOF manipulator on MATLAB Simulink with a sampling time of 0.001 seconds, and a solver of ODE3. The total simulation time is 30 seconds.

A. SIMULATION DESCRIPTIONS

FIGURE 2 presents the structure of the 2-DOF manipulator. Its dynamics parameters are shown in Appendix A. The structure of the simulation is illustrated in FIGURE 3.

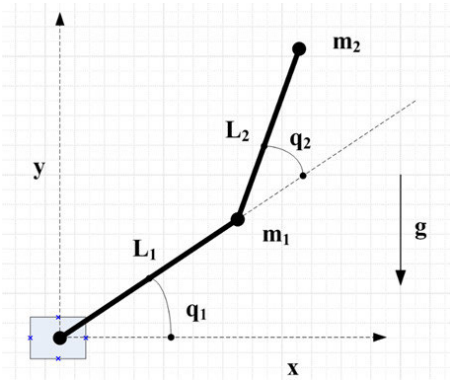

FIGURE 2. Structure of 2-DOF manipulator.

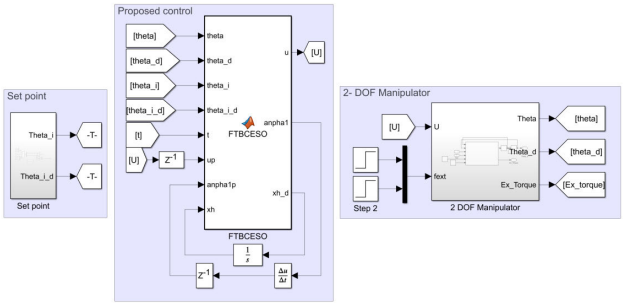

FIGURE 3. Simulation diagram.

The external uncertainties (50) consist of the friction torque and external torques caused by the external forces at the end-effector.

$$\mathbf{d}(t) = \boldsymbol{\tau}_F + \mathbf{J}^T \mathbf{F}_{ext} \tag{50}$$

The friction model, including Colomb friction and Viscous friction mode, is presented as follows:

$$\boldsymbol{\tau}_F = \mathbf{F}_v \mathbf{x}_2 + \mathbf{F}_c sign(\mathbf{x}_2) \tag{51}$$

In the last 10 seconds of the simulation period, an external force, F_x, of 5N is applied at the end-effector along the direction of the x-axis. The external force vector $F_{ext} = [F_x, 0]^T$.

TABLE 1. Coefficients of the manipulator, uncertainties, and saturation input.

Variables	Descriptions
$L_1 = 0.5(m)$	Length of link1
$L_2 = 0.4(m)$	Length of link2
$m_1 = 1.5(Kg)$	Weight of link1
$m_2 = 1(Kg)$	Weight of link1
$g = 9.81(m/s^{-2})$	Acceleration of gravity
$\mathbf{F}_c = 0.4\mathbf{I}_{2\times 2}$ (Nm)	Coefficients of Colomb friction
$\mathbf{F}_v = \mathbf{I}_{2\times 2}(Nms/rad)$	Coefficients of Viscous friction
$u_{mi} = 100Nm$	The maximum value of the ith control input

TABLE 2. Parameters of backstepping control, backstepping control with extended state observer and proposed control.

Controllers	Control parameters
BC	$\mathbf{K}_{10} = 1.3diag([108.68, 92.62])$, $\mathbf{K}_{20} = 1.3diag([4.58, 1.35])$, $\mu_0 = 1$, $\mu_\infty = 0.02$, $k_f = 0.5$, $\sigma_{11} = \pi/3$, and $\sigma_{12} = \sigma_{21} = \sigma_{22} = \sigma_{11}$
BCESO	$\mathbf{K}_{10} = 1.3diag([108.68, 92.62])$, $\mathbf{K}_{20} = 1.3diag([4.58, 1.35])$, $\mu_0 = 1$, $\mu_\infty = 0.02$, $k_f = 0.5$, $\sigma_{11} = \pi/3$, $\sigma_{12} = \sigma_{21} = \sigma_{22} = \sigma_{11}$, $\sigma_{10} = 67$, and $\sigma_{20} = 50$
Proposed control (FTBCESO)	$\mathbf{K}_{10} = diag([108.68, 92.62])$, $\mathbf{K}_1 = 0.3diag([108.68, 92.62])$, $\mathbf{K}_{20} = diag([4.58, 1.35])$, $\mathbf{K}_2 = 0.3diag([4.58, 1.35])$, $\mu_0 = 1$, $\mu_\infty = 0.02$, $k_f = 0.5$, $\sigma_{11} = \pi/3$, $\sigma_{12} = \sigma_{21} = \sigma_{22} = \sigma_{11}$, $\sigma_{10} = 67$, and $\sigma_{20} = 50$

The actuator faults arise in the manipulator as follows:

$$\begin{cases} \alpha_i = 1, & t \le 15 \\ \alpha_i = 0.6, & t > 15 \end{cases} \tag{52}$$

$$\begin{cases} \tilde{u}_i = 0, & t < 20 \\ \tilde{u}_i = 5, & t \ge 20 \end{cases} \tag{53}$$

The coefficients of the manipulator dynamics, the uncertainties, and the predefined output constraints are expressed in TABLE 1.

Additionally, a backstepping control (BC) and a backstepping control with Extended state observer (BCESO) are also

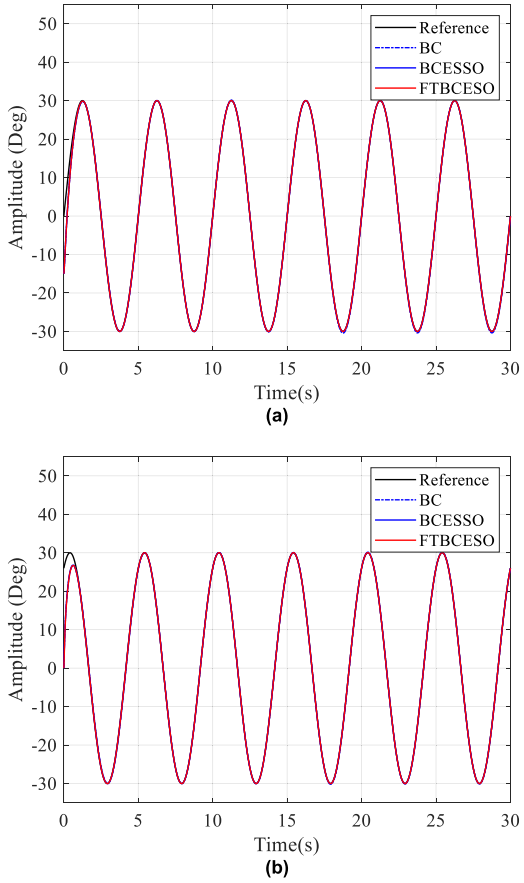

FIGURE 4. Output responses of three controllers in a) Joint 1 and b) Joint 2.

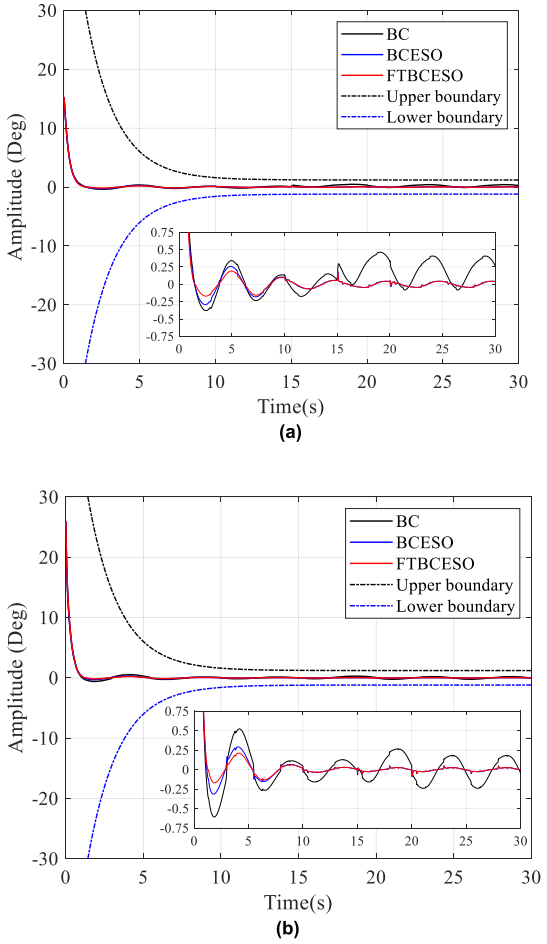

FIGURE 5. Error efforts and its zooming results of three controllers in a) Joint 1 and b) Joint 2.

conducted in these simulation scenarios, and their results will be compared with the proposed control to demonstrate the effectiveness of the proposed method. The backstepping control is designed based on the transformed manipulator dynamics (28). Its results allow us to explore the effects of the uncertainties on system stability and accuracy and the satisfaction of the predefined performances of the output responses. The control laws of this approach are presented as follows:

$$\begin{aligned} \boldsymbol{\alpha}_1 &= \mathbf{H}^{-1}\left(-\mathbf{K}_{10}\mathbf{e}_z - \boldsymbol{\Psi}\right) \\ \mathbf{u}\left(t\right) &= -\mathbf{H}\mathbf{e}_z - \mathbf{K}_{20}\mathbf{e}_2 + \mathbf{C}\left(\mathbf{x}_1, \mathbf{x}_2\right)\boldsymbol{\alpha}_1 + \mathbf{G}\left(\mathbf{x}_1\right) + \mathbf{M}\dot{\boldsymbol{\alpha}}_1 \end{aligned} \tag{54}$$

The BCESO is designed from the backstepping control (54) with an extended state observer. Then, the influences of the input faults and external disturbance to the performances of the system can be managed by the compensation signals, which are resulted by the ESO in the BCESO. The control laws of this method are expressed as follows:

$$\begin{aligned} \boldsymbol{\alpha}_1 &= \mathbf{H}^{-1}\left(-\mathbf{K}_{10}\mathbf{e}_z - \boldsymbol{\Psi}\right) \\ \mathbf{u}\left(t\right) &= -\mathbf{H}\mathbf{e}_z - \mathbf{K}_{20}\mathbf{e}_2 + \mathbf{C}\left(\mathbf{x}_1, \mathbf{x}_2\right)\boldsymbol{\alpha}_1 + \mathbf{G}\left(\mathbf{x}_1\right) \\ &\quad + \mathbf{M}\dot{\boldsymbol{\alpha}}_1 - \mathbf{M}\hat{\mathbf{x}}_3 \end{aligned} \tag{55}$$

where $\hat{\mathbf{x}}_3$ is calculated by (19).

Remark 7: The parameters of all three controllers are selected by the trial-error method. For the equality of comparisons, some parameters of the proposed control are kept from the BCESO and other of the BCESO are inherited from the BC. To save time cost in selecting control parameter process, a genetic algorithm is used to find the optimal values based on predefined criteria. The parameters of the three controllers are exhibited in IV-B.

B. PERFORMANCE CRITERIA

The following performance indexes are utilized in evaluating the quality of each control approach.

Integral square error (ISE) index:

$$ISE = \sum_k e_1^T\left(k\right) e_1\left(k\right) \tag{56}$$

Integral absolute error (IAE) index:

$$IAE = \sum_k \sum_i \left|e_{1i}\left(k\right)\right| \tag{57}$$

C. SIMULATION RESULTS

Based on the working conditions in the simulation description, the manipulator operation is divided into four stages.

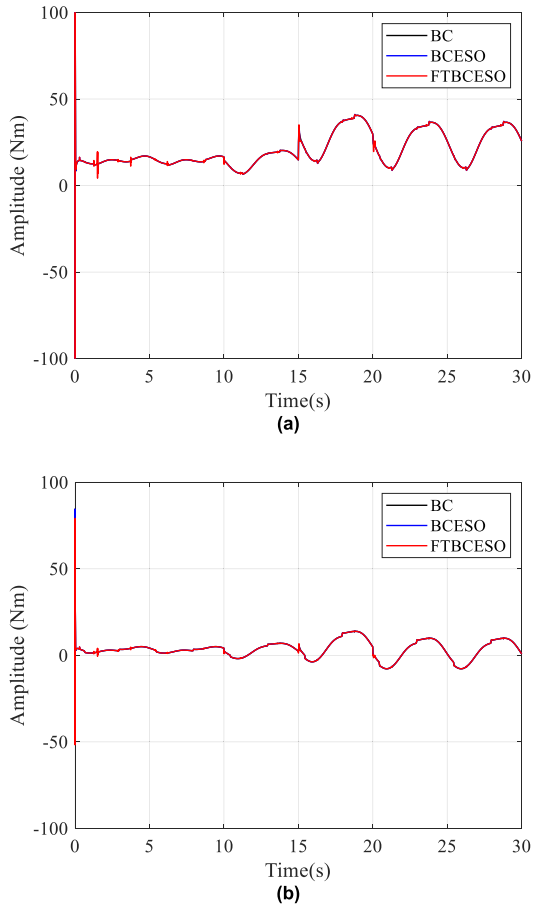

FIGURE 6. Control signals of three controllers in a) Joint 1 and b) Joint 2.

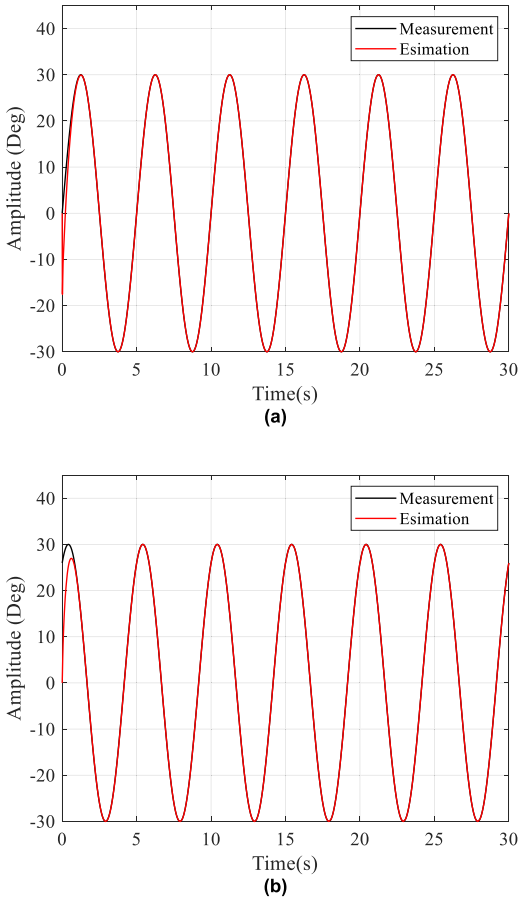

FIGURE 7. Output responses of the manipulator and the ESO in a) Joint 1 and b) Joint 2.

In the first stage, this study considers the effects of the input saturation, friction torques, and predefined performances on the output responses with three controllers. It takes place in the first 10 seconds. Next, the second stage happens in the next 5 seconds, from the 10^{th} second to 15^{th} seconds, when the external force is applied at the end-effector along the direction of the x-axis. In the third stage, from the 15^{th} second to the 20^{th} second, the loss effectiveness of actuators is considered. Finally, in the fourth stage, the bias faults are added in the manipulator from the 20^{th} second to the 30^{th} second.

FIGURE 4 presents the output responses of each joint in a 2-DOF manipulator with black lines of reference, blue dashed lines of BC, blue lines of BCESO, and red lines of the proposed control. The references are sine signals which are selected as $x_{1d} = \left[\frac{\pi}{6}\sin(2\pi ft)\ \frac{\pi}{6}\sin\left(2\pi ft+\frac{\pi}{3}\right)\right]$ (rad) with $f = 0.1\,(Hz)$. The initial positions of the two joints are set up at $x_1(0) = \left[\frac{\pi}{12}\ 0\right]^T$ (rad). The results in FIGURE 4 prove that the output responses of the controlled system with three controllers track the references under the presence of uncertainties. However, the quality of the output performances of the three controllers is different.

To evaluate the effectiveness of the proposed controllers, the error efforts at each joint are exhibited in FIGURE 5. In FIGURE 5, error performances of BC, BCESO, and

TABLE 3. Performance indexes of three controllers from the 2^{ND} second to the 30^{th} seconds.

	BC	FTBC	Proposed control
ISE index	2613	423	225
IAE index	4989	3105	2475

proposed control are displayed by black lines, blue lines, and red lines, respectively. Additionally, the upper boundaries and lower boundaries are also presented by black dashed dot lines, and blue dashed dot lines, respectively. For readability, zooming results of the error efforts in joint 1 and joint 2 are added. In the first stage, the uncertainties are friction torques. The ESO demonstrated its effectiveness in compensating the uncertainties. However, this approximation is not perfect since the ESO did not work well with the Column friction. The proposed control with the fractional terms in the control laws has driven the errors to converge to zero better than the BCESO. In the section stage, an external disturbance is applied at the end-effector of the manipulator. Because three controllers are designed based on the predefined boundaries, and these boundaries approach the steady-state, their accuracy is enhanced significantly. The proposed control is still the best solution. In the third stage, the loss efficiency faults are applied in two joints of the manipulator. The accuracy of the BC is degraded dramatically comparing other methods. By using the results of the ESO

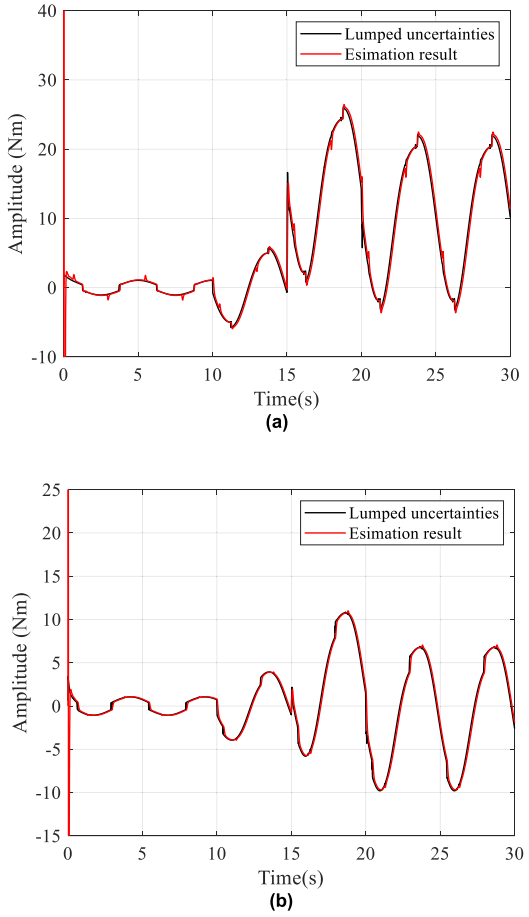

FIGURE 8. Lumped uncertainties and Estimation results of the ESO in a) Joint 1 and b) Joint 2.

to compensate for these lumped uncertainties, the BCESO and the FTBCESO still maintain the accuracy of the control system. In the final stage, the bias faults are added to the actuators. Now, the lumped uncertainties included the friction torques, the external disturbances, the loss efficiency faults, and the bias faults. The accuracy of the controlled system with the BCESO and the FTBCESO does not change. Based on the above analysis, we can conclude that the ESO can manage well with the loss efficiency and bias faults in the actuators.

FIGURE 6 present the control signals of three controllers in two joints. The BC, BCESO, and FTBCESO signals are plotted by black, blue, and red lines, respectively. When the working condition is changed in simulation time, the control signals in three controllers automatically increase to handle the lumped uncertainties and to guarantee the satisfaction of the predefined performances and the accuracy in the controlled system.

FIGURE 7 plots the measured position and the estimation position of each joint with black lines and red lines, respectively. The results show that the ESO works well when the estimated results track the measured ones. As a result, estimated lumped uncertainties in the ESO approximated the lumped uncertainties as presented in FIGURE 8.

The performance indexes of three controllers from the simulation results are shown in TABLE 3. The results of the BCESO are better than the CBC because the lumped uncertainties are compensated by the ESO in the BCESO design. Additionally, the proposed controller provides the best performance for the manipulator against the challenges. Its responses are better than the BCESO because the fractional-order terms in the controller drove the tracking error convergence in finite time.

V. CONCLUSION

This paper presented a novel finite-time fault tolerance control for an n-DOF manipulator against the actuator faults, input saturation, and external disturbance. Additionally, the proposed control guarantees that the output responses obtain the predefined performance named output constraints. To manage the above criteria with the mentioned challenges, the proposed control design is implemented on a free constrained manipulator dynamics, which is the result of integrating the output constraints into the manipulator dynamics by a transformation technique. Additionally, other problems are also described in the new manipulator dynamics. Some analysis in the paper pointed out that the predefined performance is obtained when the new dynamics are stable. Because the proposed control is constructed based on a finite-time backstepping control and an extended state observer, it not only enhances the transient time but also improves the accuracy of the controlled system. Some analyses, in theory, are conducted by the Lyapunov approach to demonstrate the effectiveness of the proposed control. Furthermore, the proposed control is implemented on a 2-DOF manipulator by MATLAB Simulink. To verify the superiority of the proposed control, its simulation results are compared to those of other controllers.

APPENDIX A

The dynamic formulation of the 2-DOF manipulator is computed by using the Euler-Lagrange approach. Because

$$\mathbf{M}(\mathbf{q}) = \begin{bmatrix} m_1 L_1^2 + m_2\left(L_1^2 + 2L_1L_2c_2 + L_2^2\right) & m_2\left(L_1L_2c_2 + L_2^2\right) \\ m_2\left(L_1L_2c_2 + L_2^2\right) & m_2L_2^2 \end{bmatrix},$$

$$\mathbf{C}(\mathbf{q}, \dot{\mathbf{q}}) = \begin{bmatrix} -m_2L_1L_2s_2\dot{q}_2 & -m_2L_1L_2s_2\dot{q}_1 - m_2L_1L_2s_2\dot{q}_2 \\ m_2L_1L_2s_2\dot{q}_1 & 0 \end{bmatrix},$$

$$\mathbf{G}(\mathbf{q}) = \begin{bmatrix} (m_1 + m_2)L_1gc_1 + m_2gL_2c_{12} \\ m_2gL_2c_{12} \end{bmatrix},$$

$$\mathbf{H} = 0.5diag\left(\left[\begin{array}{cc} \dfrac{(\sigma_{11}+\sigma_{21})\,\mu}{(e_{11}+\sigma_{21}\mu)\,(\sigma_{21}\mu-e_{11})} & \dfrac{(\sigma_{12}+\sigma_{22})\,\mu}{(e_{12}+\sigma_{22}\mu)\,(\sigma_{22}\mu-e_{12})} \end{array}\right]\right)$$

$$\mathbf{\Psi} = k_f\,(\mu_\infty-\mu_0)\,e^{-k_f t}\cdot \left[\begin{array}{cc} \dfrac{(\sigma_{11}+\sigma_{21})\,e_{11}}{(e_{11}+\sigma_{21}\mu)\,(\sigma_{21}\mu-e_{11})} & \dfrac{(\sigma_{12}+\sigma_{22})\,e_{12}}{(e_{12}+\sigma_{22}\mu_2)\,(\sigma_{22}\mu-e_{12})} \end{array}\right]^T$$

the aims of this study are evaluating the effectiveness of the proposed method with manipulators when the uncertainties impact it, we assume that all mass exists as a point mass at the distal end of each link [5]. The inertia matrix, Coriolis matrix, and Gravity vector are expressed as follows $\mathbf{M}(\mathbf{q})$, $\mathbf{C}(\mathbf{q},\dot{\mathbf{q}})$, $\mathbf{G}(\mathbf{q})$, as shown at the bottom of the previous page and

$$\mathbf{J}(q) = \left[\begin{array}{cc} -L_1 s_1 - L_2 s_{12} & -L_2 s_{12} \\ L_1 c_1 + L_2 c_{12} & L_2 c_{12} \end{array}\right]$$

where $c_i = \cos(q_i)$, $s_i = \sin(q_i)$, $c_{12} = \cos(q_1+q_2)$, and $s_{12} = \sin(q_1+q_2)$, $(i = 1, 2)$.

APPENDIX B

From the transformation function (24) and (27), the matrix, $\mathbf{H}$, and vector, $\mathbf{\Psi}$, of the 2-DOF manipulator are calculated as follows $\mathbf{H}$, $\mathbf{\Psi}$, as shown at the top of the page.

REFERENCES

[1] T. Yang, N. Sun, Y. Fang, X. Xin, and H. Chen, "New adaptive control methods for n-link robot manipulators with online gravity compensation: Design and experiments," *IEEE Trans. Ind. Electron.*, vol. 69, no. 1, pp. 539–548, Jan. 2022.

[2] A. T. Vo and H.-J. Kang, "An adaptive terminal sliding mode control for robot manipulators with non-singular terminal sliding surface variables," *IEEE Access*, vol. 7, pp. 8701–8712, 2018.

[3] Z. Chen, X. Yang, X. Zhang, and P. X. Liu, "Finite-time trajectory tracking control for rigid 3-DOF manipulators with disturbances," *IEEE Access*, vol. 6, pp. 45974–45982, 2018.

[4] S. Zhang, Y. Dong, Y. Ouyang, Z. Yin, and K. Peng, "Adaptive neural control for robotic manipulators with output constraints and uncertainties," *IEEE Trans. Neural Netw. Learn. Syst.*, vol. 29, no. 11, pp. 5554–5564, Nov. 2018.

[5] J. J. Craig, *Introduction to Robotics: Mechanics and Control*. Upper Saddle River, NJ, USA: Prentice-Hall, 2005.

[6] A. Laib, "Adaptive output regulation of robot manipulators under actuator constraints," *IEEE Trans. Robot. Autom.*, vol. 16, no. 1, pp. 29–35, Feb. 2000.

[7] W. He, X. He, M. Zou, and H. Li, "PDE model-based boundary control design for a flexible robotic manipulator with input backlash," *IEEE Trans. Control Syst. Technol.*, vol. 27, no. 2, pp. 790–797, Mar. 2019.

[8] H. Wang and S. Kang, "Adaptive neural command filtered tracking control for flexible robotic manipulator with input dead-zone," *IEEE Access*, vol. 7, pp. 22675–22683, 2019.

[9] S. Zhang, M. Lei, Y. Dong, and W. He, "Adaptive neural network control of coordinated robotic manipulators with output constraint," *IET Control Theory Appl.*, vol. 10, no. 17, pp. 2271–2278, 2016.

[10] D. T. Tran, D. X. Ba, and K. K. Ahn, "Adaptive backstepping sliding mode control for equilibrium position tracking of an electrohydraulic elastic manipulator," *IEEE Trans. Ind. Electron.*, vol. 67, no. 5, pp. 3860–3869, May 2020.

[11] S.-H. Han, M. S. Tran, and D.-T. Tran, "Adaptive sliding mode control for a robotic manipulator with unknown friction and unknown control direction," *Appl. Sci.*, vol. 11, no. 9, p. 3919, Apr. 2021.

[12] D.-T. Tran, H.-V.-A. Truong, and K. K. Ahn, "Adaptive nonsingular fast terminal sliding mode control of robotic manipulator based neural network approach," *Int. J. Precis. Eng. Manuf.*, vol. 22, no. 3, pp. 417–429, Mar. 2021.

[13] D. T. Tran, M. Jin, and K. K. Ahn, "Nonlinear extended state observer based on output feedback control for a manipulator with time-varying output constraints and external disturbance," *IEEE Access*, vol. 7, pp. 156860–156870, 2019.

[14] V.-C. Nguyen, A.-T. Vo, and H.-J. Kang, "A finite-time fault-tolerant control using non-singular fast terminal sliding mode control and third-order sliding mode observer for robotic manipulators," *IEEE Access*, vol. 9, pp. 31225–31235, 2021.

[15] D. Brambilla, L. M. Capisani, A. Ferrara, and P. Pisu, "Fault detection for robot manipulators via second-order sliding modes," *IEEE Trans. Ind. Electron.*, vol. 55, no. 11, pp. 3954–3963, Nov. 2008.

[16] Z. Gao, C. Cecati, and S. X. Ding, "A survey of fault diagnosis and fault-tolerant techniques—Part I: Fault diagnosis with model-based and signal-based approaches," *IEEE Trans. Ind. Electron.*, vol. 62, no. 6, pp. 3757–3767, Jun. 2015.

[17] M. Van, X. P. Do, and M. Mavrovouniotis, "Self-tuning fuzzy PID-nonsingular fast terminal sliding mode control for robust fault tolerant control of robot manipulators," *ISA Trans.*, vol. 96, pp. 60–68, Jan. 2020.

[18] M. Van, M. Mavrovouniotis, and S. S. Ge, "An adaptive backstepping nonsingular fast terminal sliding mode control for robust fault tolerant control of robot manipulators," *IEEE Trans. Syst., Man, Cybern. Syst.*, vol. 49, no. 7, pp. 1448–1458, Jul. 2019.

[19] Z. Wang, Q. Li, and S. Li, "Adaptive integral-type terminal sliding mode fault tolerant control for spacecraft attitude tracking," *IEEE Access*, vol. 7, pp. 35195–35207, 2019.

[20] Z. Shen, Y. Ma, and Y. Song, "Robust adaptive fault-tolerant control of mobile robots with varying center of mass," *IEEE Trans. Ind. Electron.*, vol. 65, no. 3, pp. 2419–2428, Mar. 2018.

[21] H.-B. Kang and J.-H. Wang, "Adaptive control of 5 DOF upper-limb exoskeleton robot with improved safety," *ISA Trans.*, vol. 52, no. 6, pp. 844–852, 2013.

[22] J. Yu, Y. Sun, W. Lin, and Z. Li, "Fault-tolerant control for descriptor stochastic systems with extended sliding mode observer approach," *IET Control Theory Appl.*, vol. 11, no. 8, pp. 1079–1087, May 2017.

[23] S. Huang, K. K. Tan, and T. H. Lee, "Fault diagnosis and fault-tolerant control in linear drives using the Kalman filter," *IEEE Trans. Ind. Electron.*, vol. 59, no. 11, pp. 4285–4292, Nov. 2012.

[24] Y. S. Hagh, R. M. Asl, and V. Cocquempot, "A hybrid robust fault tolerant control based on adaptive joint unscented Kalman filter," *ISA Trans.*, vol. 66, pp. 262–274, Jan. 2017.

[25] M. Van, S. S. Ge, and H. Ren, "Finite time fault tolerant control for robot manipulators using time delay estimation and continuous nonsingular fast terminal sliding mode control," *IEEE Trans. Cybern.*, vol. 47, no. 7, pp. 1681–1693, Jul. 2017.

[26] A. Zhang, C. Lv, Z. Zhang, and Z. She, "Finite time fault tolerant attitude control-based observer for a rigid satellite subject to thruster faults," *IEEE Access*, vol. 5, pp. 16808–16817, 2017.

[27] Q. D. Le and H.-J. Kang, "Finite-time fault-tolerant control for a robot manipulator based on synchronous terminal sliding mode control," *Appl. Sci.*, vol. 10, no. 9, p. 2998, Apr. 2020.

[28] M. Lingya and J. Bin, "Backstepping-based active fault-tolerant control for a class of uncertain SISO nonlinear systems," *J. Syst. Eng. Electron.*, vol. 20, no. 6, pp. 1263–1270, 2009.

[29] Y. Yi and D. Chen, "Disturbance observer-based backstepping sliding mode fault-tolerant control for the hydro-turbine governing system with dead-zone input," *ISA Trans.*, vol. 88, pp. 127–141, May 2019.

[30] Q. Guo, Y. Zhang, B. G. Celler, and S. W. Su, "Neural adaptive backstepping control of a robotic manipulator with prescribed performance constraint," *IEEE Trans. Neural Netw. Learn. Syst.*, vol. 30, no. 12, pp. 3572–3583, Dec. 2019.
[31] S. I. Han and J. M. Lee, "Improved prescribed performance constraint control for a strict feedback non-linear dynamic system," *IET Control Theory Appl.*, vol. 7, no. 14, pp. 1818–1827, Sep. 2013.
[32] Y. Yang, J. Tan, and D. Yue, "Prescribed performance control of one-DOF link manipulator with uncertainties and input saturation constraint," *IEEE/CAA J. Automatica Sinica*, vol. 6, no. 1, pp. 148–157, Jan. 2019.
[33] K. P. Tee, S. S. Ge, and E. H. Tay, "Barrier Lyapunov functions for the control of output-constrained nonlinear systems," *Automatica*, vol. 45, no. 4, pp. 918–927, Apr. 2009.
[34] D. T. Tran, H. V. Dao, H. Liu, Y. J. Yum, and K. K. Ahn, "Barrier Lyapunov function based output control and extended state observer for a manipulator with time-varying output constraints and uncertainties," in *Proc. 23rd Int. Conf. Mechatronics Technol. (ICMT)*, Oct. 2019, pp. 1–6.
[35] Y. Wu, R. Huang, X. Li, and S. Liu, "Adaptive neural network control of uncertain robotic manipulators with external disturbance and time-varying output constraints," *Neurocomputing*, vol. 323, pp. 108–116, Jan. 2019.
[36] K. P. Tee, B. Ren, and S. S. Ge, "Control of nonlinear systems with time-varying output constraints," *Automatica*, vol. 47, no. 11, pp. 2511–2516, Nov. 2011.
[37] Y.-J. Liu, S. Lu, S. Tong, X. Chen, C. L. P. Chen, and D.-J. Li, "Adaptive control-based Barrier Lyapunov Functions for a class of stochastic nonlinear systems with full state constraints," *Automatica*, vol. 87, pp. 83–93, Jan. 2018.
[38] W. Wang and C. Wen, "Adaptive actuator failure compensation control of uncertain nonlinear systems with guaranteed transient performance," *Automatica*, vol. 46, no. 12, pp. 2082–2091, 2010.
[39] J. Yu, P. Shi, and L. Zhao, "Finite-time command filtered backstepping control for a class of nonlinear systems," *Automatica*, vol. 92, pp. 173–180, Jun. 2018.
[40] S. M. Smaeilzadeh and M. Golestani, "Finite-time fault-tolerant adaptive robust control for a class of uncertain non-linear systems with saturation constraints using integral backstepping approach," *IET Control Theory Appl.*, vol. 12, no. 15, pp. 2109–2117, 2018.
[41] D. T. Tran, H. V. Dao, T. Q. Dinh, and K. K. Ahn, "Output feedback control via linear extended state observer for an uncertain manipulator with output constraints and input dead-zone," *Electronics*, vol. 9, no. 9, p. 1355, Aug. 2020.

DUC THIEN TRAN (Member, IEEE) received the B.S. and M.S. degrees from the Department of Electrical Engineering, Ho Chi Minh City University of Technology, Vietnam, in 2010 and 2013, respectively, and the Ph.D. degree from the University of Ulsan, in 2020.

He currently works as a Lecturer with the Department of Automatic Control, Ho Chi Minh City University of Technology and Education (HCMUTE), Vietnam. His research interests include robotics, variable stiffness systems, fluid power control, disturbance observer, nonlinear control, adaptive control, and intelligent technique.

KYOUNG KWAN AHN (Senior Member, IEEE) received the B.S. degree from the Department of Mechanical Engineering, Seoul National University, in 1990, the M.Sc. degree in mechanical engineering from the Korea Advanced Institute of Science and Technology (KAIST), in 1992, and the Ph.D. degree from the Tokyo Institute of Technology, in 1999.

Since 2000, he has been with the School of Mechanical Engineering, University of Ulsan, where he is currently a Professor and the Director of the Fluid Power Control and Machine Intelligence Laboratory. His main research interests include fluid-based triboelectric nano generator, modeling and control of fluid power systems, energy saving construction machine, hydraulic robot, and power transmission in the ocean energy. He is the author or coauthor of over 190 SCI(E) articles and four books in these areas.

Dr. Ahn serves as an Editor for the *International Journal of Control, Automation and Systems* and an Editorial Board Member of *Renewable Energy*, *Korean Fluid Power and Construction Machine*, and *Actuators*.